Ultrafast Diagnostics for Electron Beams from Laser Plasma Accelerators

N. H. Matlis, M. Bakeman, C. G. R. Geddes, T. Gonsalves, C. Lin, K. Nakamura, J. Osterhoff, G. R. Plateau, C. B. Schroeder, S. Shiraishi, T. Sokollik, J. van Tilborg, Cs. Tóth, W. P. Leemans

Lawrence Berkeley National Laboratory, 1 Cyclotron Rd., Berkeley, CA 94720

Abstract. We present an overview of diagnostic techniques for measuring key parameters of electron bunches from Laser Plasma Accelerators (LPAs). The diagnostics presented here were chosen because they highlight the unique advantages (e.g. diverse forms of electromagnetic emission) and difficulties (e.g. shot-to-shot variability) associated with LPAs. Non destructiveness and high resolution (in space and time and energy) are key attributes that enable the formation of a comprehensive suite of simultaneous diagnostics which are necessary for the full characterization of the ultrashort, but highly-variable electron bunches from LPAs.

Keywords: THz, Wakefield, Laser, Plasma, Accelerator, Diagnostic
PACS: 52.25.Os, 52.38.-r, 52.38.Kd, 78.20.Jq, 78.47.J-, 07.77.Ka, 29.27.Fh

INTRODUCTION

Laser Plasma Accelerators (LPAs) are becoming increasingly important as compact sources of high-energy electrons. As this technology begins to mature, a wide variety of applications, from high-energy colliders to free-electron lasers [1], are emerging that would benefit greatly from it, spurring interest. The primary limitations of these accelerators impeding their application in general include their lack of shot-to-shot stability and the lack of fine-tuning of the beam parameters. A crucial step that precedes the ability to fine-tune and stabilize the electron beam parameters, however, is the ability to measure them. As a result, a significant focus of LPA research has been dedicated to the development of diagnostic techniques [2]. While the field of electron beam diagnosis in conventional accelerators is very mature, LPAs have several unique features that require evaluation of the suitability of the conventional techniques to this new accelerator format, as well as development of new ones. One of the most notable and promising features of LPAs is their ability to produce electron bunches of extremely short durations, which are expected to be in the few femtosecond regime. While such short durations are very desirable for many applications, they can be exceptionally difficult to measure, requiring development of new methods with ultrahigh temporal resolution. The susceptibility of LPAs to shot-to-shot fluctuations in the beam parameters is their other salient feature. Because of this high variability, it is generally not practical to measure the various beam parameters in series on separate shots. It is thus critical to the advancement of LPA sources to develop a full suite of diagnostics which can be run simultaneously in a single-shot. This requirement implies the necessity of non-destructiveness in these diagnostics. Here we present an overview of several diagnostics which can be used in parallel to measure charge, energy, energy spread, emittance, and longitudinal and transverse structure of the electron beams from LPAs. Much advantage is taken of electromagnetic emission from the accelerated electrons produced through various mechanisms, some of which are byproducts of the acceleration process.

CHARGE DIAGNOSTICS

Integrating Current Transformers (ICTs) have become standard instruments for the measurement of charge in conventional accelerators because of their ease of use, precision and non invasiveness. More recently, ICTs have been critical tools for the LPA community as well. Because of the importance of accurate absolute charge measurement for a large number of labs (including medical institutions), many tests have been done to verify the accuracy of ICTs for electron bunches with durations typical for conventional accelerators. No bunch-length dependence has yet

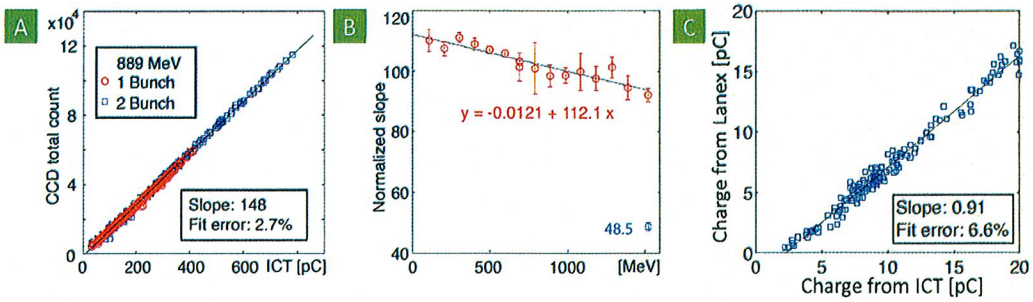

FIGURE 1. Comparison of ICT-based and Lanex-based charge measurements. Courtesy of Nakamura et al. [6].

been reported in the range from microseconds down to picoseconds [3], but the regime of fs bunches has remained unconfirmed. Two recent studies [4, 5] reported discrepancies between charge measurements done with ICTs and scintillating screens, questioning the suitability of ICTs for use in LPAs. In the first experiment [4], discrepancies of greater than an order of magnitude, were observed. These discrepancies were attributed to the following potential problems: (1) that the ICT was not designed to measure sub-100 fs bunches, (2) the effect of electrons passing outside the core was not known, (3) that the electronic system was susceptible to electromagnetic noise generated in the interaction, and (4) that the ICT is sensitive to the large amount of low energy charge emitted at wide angles. In the second experiment [5], the ICT was found to overestimate the scintillating screen-based measurement by a factor of $3-4$. The importance of ICTs to the LPA community combined with the doubt cast on them by these studies provides strong motivation for further detailed investigation into the applicability of ICTs to charge diagnosis in the harsh LPA environment.

A detailed series of experiments was recently done to cross-calibrate ICT-based charge measurement with two alternate methods of charge measurements based on scintillating screens (Lanex) and nuclear activation of a copper target [6]. In these experiments, the light yield from the Lanex screen was first calibrated using the electron beams provided by the synchrotron booster ring at the Advanced Light Source at Lawrence Berkeley National Lab (LBNL) in an energy range from $0.1-1.5$ GeV (Fig. 1a, 1b). A slight dependence of the light yield on electron energy was observed at the 1% per 100 MeV level. Subsequently, an experiment was carried out on the LPA system at the LOASIS facility, LBNL using the three detection systems. Multiple steps were taken to ensure the accuracy of the comparison: 1) electronic noise was mitigated by using well-shielded cables, and the length of the cables was chosen in order to temporally separate the signal from the noise generated by the interaction; 2) the ICT was installed outside the vacuum tube, over a ceramic spacer to avoid the effects of electrons and laser light impacting the ICT; 3) the ICT was placed close to the Lanex screen, and an aperture was used to ensure a common angular acceptance for both detectors to avoid errors induced by the effect of large divergences of lower energy electrons; 4) the ICT and Lanex were placed sufficiently far from the interaction to ensure that a small residual magnetic field of $\sim$ 0.4 mT would be sufficient to deflect keV electrons to which the Lanex screen may be insensitive. Comparison of the Lanex and ICT measurements shows agreement to within $\sim$ 9% (Fig. 1c) for bunch charges ranging from $0-20$ pC. Analysis of the nuclear activation experiment likewise resulted in agreement with the ICT to within $\sim$ 7%, for charge integrated for over an hour. The good agreement between these three measurements demonstrates that there is no intrinsic limitation of ICTs preventing their use in LPA systems. The previously reported discrepancies, however, indicate the importance of accounting for effects common to LPAs, such as the strong dependence of bunch divergence on electron energy, and of taking the proper measures to ensure reliable operation.

UNDULATOR EMISSION

One promising application of LPAs is the development of compact free electron lasers (FELs) as ultrashort sources of electromagnetic radiation from THz to x-rays [7, 8]. The high peak currents and ultrashort bunch durations of LPA electron bunches are ideal for the generation of high-brightness, coherent, short-wavelength radiation desirable for a wide range of studies, such as the reconstruction of the structure of complex biological molecules. The synchrotron

spectrum of FEL undulators, however, is extremely sensitive to the energy, energy spread and emittance of the electron bunches injected, posing severe conditions on LPAs. This difficulty, on the other hand, becomes an advantage if the emission spectrum is used as a diagnostic of the electron bunches [9, 10, 11]. The current state-of-the-art for measuring the energy-spectrum of the accelerated electrons is the use of an imaging magnetic spectrometer. In these devices, a tunable magnetic field images and spectrally disperses the electrons in one plane. Scintillating screens (e.g. Lanex) are then used to measure the distribution of charge in the Fourier plane of the spectrometer, providing single-shot information of the energy distribution of the electrons emitted by the accelerator. This approach is ideal for LPAs because it provides single-shot detection over a large range of energies, allowing diagnosis of both the low-energy Maxwellian tail of the bunch as well as the high-energy "quasi-monoenergetic" component of the beam. The drawback of this method is that in order to resolve the full range of energies, from MeV to GeV, the energy resolution of the device may be limited, especially at higher energies where the dispersion is smallest, resulting in resolutions on the order of a couple percent or more [12].

As progress in LPA development proceeds and researchers succeed in pushing down the energy spread of the high-energy (GeV level), mono-energetic component to the few percent level and below [13], the measured energy spreads can become resolution limited. In addition to this limitation, these devices do not provide a measurement of the beam emittance, which is critical for many applications. A powerful technique based on the characterization of undulator radiation, however, can provide both high-resolution ($< 0.1\%$ rms [14]) energy spread *and* emittance measurement on a single-shot basis [9, 2, 10, 11]. The output of an undulator is characterized by harmonics of a fundamental frequency given by [15]:

$$\omega_0 = \frac{4\pi c\gamma^2}{L_u}\left[1+\frac{K^2}{2}+\gamma^2\theta^2\right]^{-1} \tag{1}$$

where L_u is the undulator periodicity, $K = eB_0L_u/2\pi mc$ is the strength parameter, γ is the Lorentz factor for the oscillating electrons, and θ is the angle of the electron trajectory with respect to the axis of the undulator. Thus, for a given set of undulator parameters L_u and K, the on-axis contribution to the bandwidth of the n_{th} harmonic peak will be linearly dependent on the energy spread: $d\omega_n = (n\omega_0/\gamma)d\gamma$. In addition, the angular distribution of odd harmonics has a maximum at $\theta = 0$, while even harmonics have an emission pattern with a zero at $\theta = 0$. Electrons propagating along the undulator axis do not contribute to the even harmonics while electrons propagating off-axis do. The ratio of even to odd harmonic intensities therefore gives us a measure of the angular spread of the electron bunch, which, coupled with knowledge of the bunch source size, provides a measure of the emittance. Simulations done using the code SPECTRA [16] for electron bunches with varying energy spread and emittance confirm the dependence of undulator spectral features on energy and emittance (Fig. 2). Experiments are currently under way to test this concept [14, 17].

BETATRON X-RAY EMISSION

Synchrotron emission is also emitted during interaction of the electrons with the wakefield and can be used to gain information about the acceleration process itself. Electrons injected off-axis into the wakefield experience an ion channel which provides radial forces causing betatron oscillations. The oscillations occur with amplitudes on the scale of few to hundreds of microns, determining the size of the electron bunch, and resulting in emission of soft X-rays in the few keV range, known as betatron radiation. The amplitude and periodicity of the betatron oscillations depend sensitively on the shape of wakefield, the physics of the injection, and the presence of strong E-fields from the drive laser, thus the betatron x-rays can provide valuable insight into the nature of the interaction between the laser, the electrons and the plasma. In addition, as the betatron oscillation period is much shorter than that which can be achieved using external undulators, betatron x-rays from LPAs hold promise as a compact source of radiation in the keV energy range.

The betatron radiation can be characterized by a strength parameter analogous to the "K" of an undulator: $a_\beta = \gamma r_\beta \omega_\beta/c$, where $2r_\beta$ is the oscillation amplitude, $\omega_\beta = \omega_p/\sqrt{2\gamma}$ is the betatron oscillation frequency, ω_p is the plasma frequency and c is the speed of light. Various groups have demonstrated the detection of betatron radiation from LPAs, and have shown correlations of the spectra with parameters of the accelerator e.g. [18, 19, 20]. An important result that has come from these measurements is the determination of the source size of the x-rays, which was accomplished by placing knife-edges or wire meshes in the x-ray beams and observing the sharpness of the shadow cast on an imaging detector. Source sizes varying from $\sim$2 μm to several hundred microns have been measured in different conditions. As the source size is correlated to the oscillation amplitude, r_β, which is correlated to the transverse size of the electron bunch, this technique provides valuable information about the physics of the acceleration and the

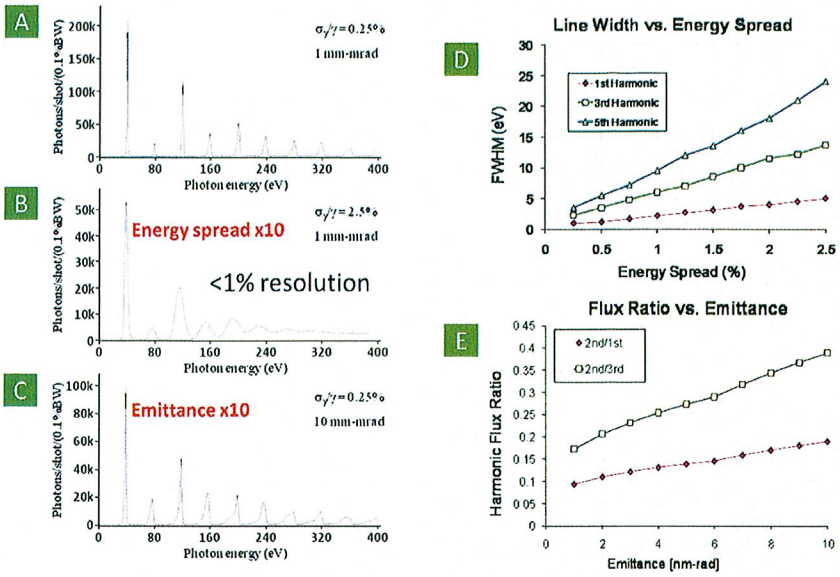

FIGURE 2. (A) Radiation spectrum from THUNDER undulator, K=1.85, $\lambda_{period} = 2.18\ cm$, energy spread = 0.25%, emittance = 1 mm.mrad, Calculated using *SPECTRA*. (B) Spectrum for 10-fold increase in energy spread. (C) Spectrum for 10-fold increase in emittance. (D) Dependence of harmonic line-width on energy spread. (E) Ratios of 2^{nd} to 1^{st} and 2^{nd} to 3^{rd} harmonic intensities as a function of the emittance. Courtesy of Bakeman et al. [10]

quality of the accelerator. These measurements also provide precise information about the shot-to-shot variation in the emission point of the electrons, which can be used to determine the stability of the accelerator. In addition, because the spectrum of the x-ray emission is dependent on both the electron density of the plasma and the energy of the accelerated electrons, it can be used as a probe of the acceleration physics (e.g. [19, 21]).

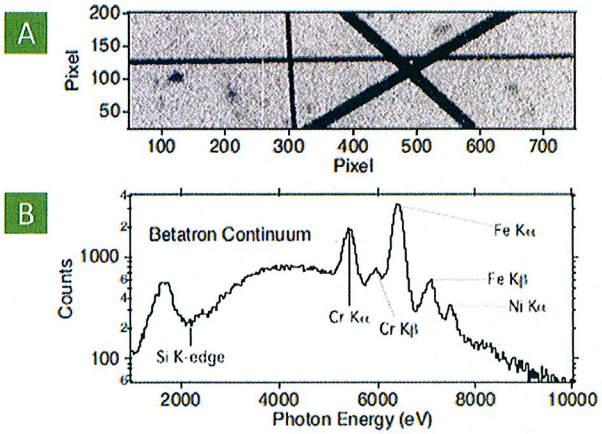

FIGURE 3. Betatron radiation from the LOASIS LPA back lighting 2 pairs of crossed wires of diameter 12.5 μm and 50 μm Courtesy of Thorn et al. [18].

Spectral measurements have previously been done in a multi-shot configuration in which the variation in x-ray yield was observed as a function of different filters placed in front of the detector. This approach is time-consuming, provides

low spectral resolution, and cannot be used to correlate individual x-ray spectra with associated electron spectra.

In a recent report [18] a technique was implemented to record measurements of single-shot, spatially-resolved spectra of betatron x-rays with high spectral resolution, by the use of an x-ray CCD. Images analyzed by performing a histogram of single-pixel absorption events (SPAE) [21] produced x-ray spectra with an unprecedented resolution of 225 eV, FWHM, and a range of over 10 keV. A source emitting iron k-shell x-ray lines was used to provide a calibration of the energy per pixel count. Preliminary data show two important features not previously resolved. The first is iron and chromium fluorescence lines associated with the interaction of electrons and x-rays with the stainless steel of the vacuum chamber, and the second is the betatron continuum. The ratio of the amplitude of the fluorescence lines to that of the betatron continuum was found to vary significantly with changes in the accelerator parameters, calling into question the validity of previous spectral analyses, based on filter packs, which cannot distinguish between these two components.

ELECTRO-OPTIC DIAGNOSTICS

Electro-optic (EO) sampling has become a widely-used technique for the measurement of electron-bunch durations and temporal structure. In this technique, either the relativistic Coulomb fields of the electron bunch or coherent transition radiation (CTR) in the THz frequency band emitted by the electron bunch traversing a dielectric boundary is used to induce birefringence in an electro-optically active crystal, such as gallium phosphide (GaP) or zinc telluride (ZnTe). An optical probe, timed to overlap with these strong electric fields, is used to sample the temporal profile of the fields, from which the duration of the electron bunch can be deduced. This technique is very powerful because it can be used in configurations that are non- or weakly-interacting with the electron bunch, allowing it to be used in conjunction with other diagnostics. In addition, it provides the high temporal resolutions required for measuring the sub-picosecond electron bunches produced in LPAs. The EO sampling process can be split into two conceptual parts: generation of the temporally-varying birefringence, and sampling of the birefringence. Three prominent methods for each will be discussed.

Generating the birefringence. In the first method (Direct Coulomb Sampling), the EO crystal is placed near to the path of the accelerated electrons, so that the Coulomb fields penetrate it, resulting in a transient birefringence. An optical probe pulse, propagating parallel to the beam line overlaps the induced fields in the crystal, and is imprinted with the temporal profile of these fields. Due to relativistic contraction, the Coulomb field profiles will be longitudinally compressed by an amount dependent on the electron energy. The field temporal profile will thus be a convolution of the charge profile with the longitudinal extent, $\tau_e = y/c\gamma$, of the electron Coulomb fields, where y is the transverse distance from the beam axis. Provided the electrons are sufficiently energetic (γ large) and the crystal is sufficiently close (y small), the field profile will represent the bunch profile well. In general, however, a polychromatic electron bunch will have a field profile (at the crystal) significantly different than its charge profile, with the lower energy electrons having a longer longitudinal field-extent than the high-energy components. At a distance of 1 mm, for example, the convolution factor will be approximately 1.7 ps for a 1 MeV component while it will be about 1.7 fs for a 1 GeV component. In addition, since the field-strength scales as γ, the EO signal will be strongly biased towards the high-energy component of the electron bunch. In scenarios where it is the behavior of the high-energy component that is of interest, such as in the FEL application, this bias can be advantageous, whereas if it is the actual longitudinal charge distribution that is desired, this approach may not be suitable. In RF accelerators (e.g. [22, 23]) where this technique has been demonstrated, the electron bunches have sufficient energy and spectral purity that this issue is not of great importance, however, for LPAs, where polychromaticity over a large energy range is often the norm (even in "quasi-monoenergetic" electron beams, where a low-energy component has a large relative charge), the error in the measurement of the longitudinal charge profile may be large.

In the second method (Foil CTR Sampling), a foil is placed in the path of the electrons resulting in the generation of transition radiation (TR) caused by transient currents in the foil induced by the passage of the electric-field profile of the electron bunch. The TR is collected and focused into an EO crystal where it generates a transient birefringence sampled with an optical probe. The spectrum of the TR is correlated to the temporal profile of the electron bunch [24] due to a strong coherent enhancement for wavelengths longer than the duration of the electron bunch. The spectral shape can thus be used to analyze the bunch longitudinal profile. In this case, the dependence of the collected CTR energy is relatively weak on the γ of the electrons, so energy-biasing is minimal. A strong dependence of the angular distribution of the CTR energy with wavelength, however, means that a correct analysis of the CTR spectrum must take into account the spectrally-dependent collection efficiency of the optical system. In addition, since the range of collected frequencies can be very large, the variation in effective f-number and focus size with wavelength can be very

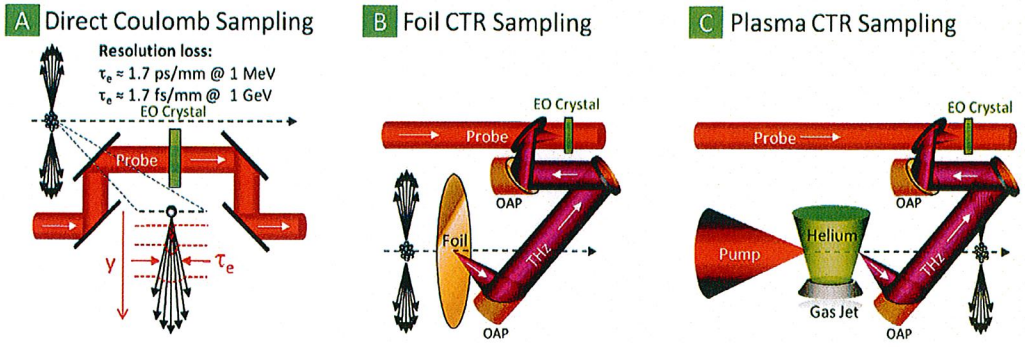

FIGURE 4. Setups for sampling (A) bunch Coulomb fields (B) CTR from a foil (C) CTR from a plasma-vacuum interface.

significant, leading to a reshaping of the spectrum at focus compared to the collection point [25]. Finally, aberrations in the optical system may induce distortions which can produce artifacts in the measurement [26].

In the third method (Plasma CTR Sampling), CTR is collected directly from the plasma-vacuum interface at the exit of the acceleration region [27]. This method is very similar to Foil CTR Sampling, except that there is no foil to interact with the electrons, so it is truly non-destructive; the collection is off-axis, avoiding the high-intensity of the transmitted laser; and the CTR is collected directly from the output of the accelerator, ensuring that there is no bunch expansion before the measurement. Although the plasma-vacuum boundary is not as sharp a discontinuity as a foil, it can be adequately modeled as a sharp boundary provided the region emitting the CTR is smaller than a distance known as the "formation length" [28].

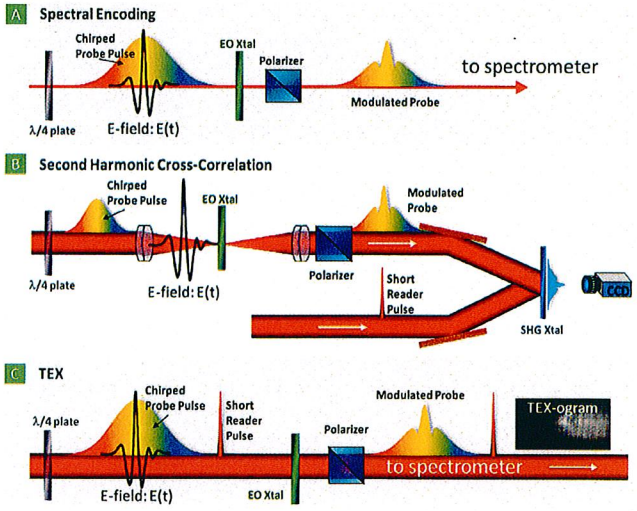

FIGURE 5. (A) Spectral Encoding (B) Second Harmonic Cross-correlation (C) Temporal Electric-field Cross-correlation (TEX).

Sampling the birefringence. Early methods for sampling the birefringence employed an optical pulse shorter than the features to be measured, i.e. the wavelength/duration of the E-field. The polarization rotation was converted to an amplitude modulation by a polarizer, and the intensity variation was recorded using a photodiode. Due to the highly variable nature of LPAs, and hence of the fields to be profiled, a multishot approach results in a washing out of the higher-frequency features which contain information about the bunch duration. As a result, a high priority is placed on the ability to perform single-shot acquisition of the field profiles. The first technique created to do this was known as "Spectral Encoding" [29]. In this technique, the optical probe was sent through a dispersive element

(e.g. a compressor/stretcher) resulting in temporal chirp, i.e. a mapping between wavelength and time. The transient birefringence was then encoded as a spectral amplitude modulation that could be measured in a spectrometer. This technique is exceptionally easy to set up, and allows for a tunable detection window by adjusting the amount of chirp. Unfortunately, the wavelength-to-time mapping is affected by the amplitude modulation, resulting in distortions [30, 31, 32]. The severity of these distortions is dependent on the sharpness of the feature being measured, so this technique is more suited to measurements with low temporal resolution (e.g. in the picosecond regime).

The second method was developed to overcome the limitations of *Spectral Encoding*. In this technique, a second short optical pulse is combined with the chirped probe in a single-shot cross-correlator geometry. The two pulses are combined at an angle in a second harmonic crystal, mapping time to space, resulting in a spatial intensity pattern that is the cross-correlation of the temporal envelopes of the chirped probe and short reference [33, 34]. The spatial intensity pattern can then be measured using a CCD camera, and the corresponding temporal profile can be determined using the appropriate calibration. This method has been successfully used in both conventional accelerators [23] and in LPAs [33] to measure electron bunch profiles with high temporal resolution (10s of fs). This technique, however, has the disadvantage that it requires high probe intensities, and thus expensive amplified lasers in order to get adequate signal. In addition, because the temporal signal is encoded spatially and the probe laser is focused at the interaction, spatial information about the THz pulses is lost. As the THz pulses in many of these applications are few-cycle, with ultrabroad bandwidths, focused THz waveforms (which are often few-cycle) can exhibit strong spatiotemporal coupling due to Gaussian beam propagation effects associated with ultra-broad bandwidths [35]. Failure to resolve the spatial variations can therefore result in a loss of critical information.

A new technique named Temporal Electric-field Cross-correlation (TEX) has been developed which overcomes the above limitations, allowing measurement of THz waveforms with high temporal resolution (sub-50 fs), simultaneously providing one dimension of spatial information [25]. TEX is based upon measurement of the linear cross-correlation of a chirped probe with a compressed reference pulse using spectral interferometry. The full electric-field information of the optical probe, convolved with that of the short reference, is retrieved in the time domain, allowing signals to be encoded onto either the phase or the amplitude of the probe or both. This dual capability is not present in previous EO methods, and makes TEX applicable to the measurement of a wide range of phenomena beyond EO sampling. Because the detection is linear, TEX can be implemented with low-cost, unamplified laser systems, and because it does not require focusing of the optical probe, spatial information can be recorded and retrieved. In addition, the temporal detection window is easily tunable in the several ps range, with fs temporal resolution set by the duration of the short reference pulse.

In TEX, a chirped "probe" pulse samples the birefringence and is then combined colinearly with a second short "reader" pulse in an imaging spectrometer. A temporal separation of several picoseconds between the two pulses (which have identical spectral content preceding the interaction) causes an interference pattern in the spectral domain (Fig. 6A) which is described by $S(\omega,y) = |E_p(\omega,y)|^2 + |E_r(\omega,y)|^2 + E_p(\omega,y)E_r^*(\omega,y) + c.c.$ where $E_p(\omega,y)$ and $E_r(\omega,y)$ are the spectral electric-fields of the *probe* and *reader* pulses, ω is the optical frequency and y represents the vertical, undispersed coordinate on the CCD. The *probe* amplitude and phase structure is recovered by performing a line-by-line, Fourier-transform (FT) of the interferogram and isolating the side peak which, by the convolution theorem of FTs, is the complex convolution of the *probe* and *reader* electric fields in the time domain. For a suitably short *reader* pulse, the side peak of the FT approximates the chirped probe pulse in both amplitude and phase.

$$FT[E_p(\omega,y)E_r^*(\omega,y)] = \int_{-\infty}^{\infty} E_p(\tau,y)E_r^*(\tau - t,y)d\tau \approx E_p(t,y) \tag{2}$$

Figure 6E shows a sample THz spatiotemporal waveform image acquired using TEX to sample *plasma CTR* in the amplitude-encoding configuration. The measured waveform is nearly single cycle, and displays sharp temporal features of order 100 fs, illustrating the need for high temporal resolution. The waveform also exhibits strong spatiotemporal coupling, in the shape of an **X**, as was described by Jiang et al. [35], which can be understood in terms of a variation of the Gouy phase shift and focused-waist size with wavelength. To diagnose the structure of the electron bunch, the spectrum of the THz waveform was calculated (Fig. 6G) and compared with theory (Fig. 6H). The spatial and temporal features of the spectral image were modeled by using CTR emission theory [24] with the inclusion of collection and propagation effects. To accurately model both the low- and high-frequency parts of the spectral image, two bunches of different duration and charge (90% of the charge in a 140 μm-*rms* bunch and 10% in a 50 μm bunch) were required (Fig. 6I), with the shorter bunch contributing primarily on-axis. The electron energy spectrum, measured simultaneously, also shows a two-component distribution with a large thermal- and a smaller "quasi mono-energetic" component. The importance of recovering the spatial variations in the THz waveforms is illustrated by the strong

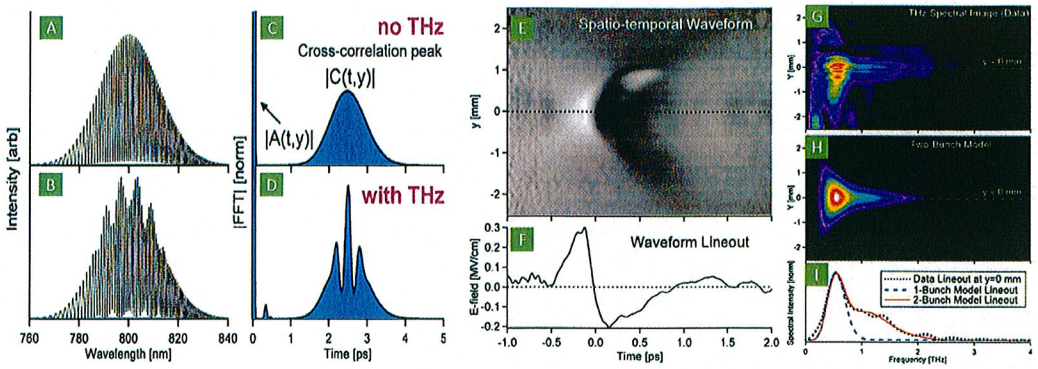

FIGURE 6. (A) Simulated TEX interferogram in the absence of THz for *probe* and *reader* pulses separated in time by 2.5 ps. (B) Simulated TEX interferogram with THz present. (C) Modulus of the Fourier transform of the interferogram in (A) showing a broad side peak at 2.5 ps which represents the amplitude of the cross-correlation between the *probe* and *reader* electric-fields. (D) Modulus of the complex Fourier transform of the interferogram in (B), showing a THz-induced modulation in the side peak amplitude. (E) THz spatiotemporal waveform (data) extracted from the raw interferogram. (F) lineout of waveform at $y = 0$ mm, (G) Power spectrum of THz waveform. (H) Spectral image calculated using a 2-bunch model and (I) lineouts of spectral images for data (black-dotted line), 1-bunch model (blue-dashed line) and 2-bunch model (red-solid line). Comparison shows that a 2-bunch model yields a significantly better fit than a 1-bunch model. Courtesy of Matlis et al. [25].

variation with position of spectral content in the focused THz pulse. A spatially-integrated technique would under-represent the high-frequency content of the THz spectrum associated with the shorter electron bunch component, thus distorting the analysis. In addition, because the spatial extent of a given spectral component is strongly dependent on both the wavelength *and* the wavelength-dependent f-number of the THz emission, the correspondence between the data and the model provides an important confirmation that the collected THz follows the emission patterns predicted by CTR theory, verifying its origin.

CONCLUSION

We have presented a suite of diagnostics, designed to handle the advantages and disadvantages inherent in LPAs compared to conventional RF accelerators. The diagnostics have been chosen because they provide non-destructive measurement of the key attributes of the accelerated electron bunches in a single-shot format. These diagnostics include ICTs for charge measurement; undulators for energy, energy spread and emittance measurement; betatron x-rays for source size measurement; and electro-optic sampling using TEX to sample CTR from the plasma-vacuum interface for electron bunch temporal profile measurement. Formation of a comprehensive suite of diagnostics to measure the attributes of the electron bunches in a single-shot is a critical step for enabling the studies of the complex interdependence of beam properties which will help drive the field of laser plasma acceleration to maturity.

ACKNOWLEDGMENTS

This work was supported by the Director, Office of Science, Office of High Energy Physics, of the U.S. Department of Energy under Contract No. DE-AC02-05CH11231, DARPA, DTRA and NA-22.

REFERENCES

1. W. P. Leemans, and E. Esarey, *Phys. Today* **62**, 44 (2009).
2. P. Catravas, E. Esarey, and W. P. Leemans, *Phys. Plasmas* **9**, 2428 (2002).
3. J. Bergoz, Integrating current transformer (ict) pulse charge accuracy, Technical Note ICT / 06.1, Bergoz Instrumentation (2006).

4. Y. Clinec, J. Faure, A. Guemnie-Tafo, V. Malka, H. Monard, J. P. Larbre, V. D. Waele, J. L. Marignier, and M. Mostafavi, *Rev. Sci. Instrum.* **77**, 103301 (2006).
5. B. Hidding, G. Pretzler, M. Clever, F. Brandl, F. Zamponi, A. Lübcke, T. Kämpfer, I. Uschmann, E. Förster, U. Schramm, R. Sauerbrey, E. Kroupp, L. Veisz, K. Schmid, S. Benavides, and S. Karsch, *Rev. Sci. Instrum.* **78**, 083301 (2007).
6. K. Nakamura, A. J. Gonsalves, C. Lin, T. Sokollik, A. Smith, D. Rodgers, R. Donahue, W. Bryne, and W. P. Leemans, "Charge Diagnostics for Laser Plasma Accelerators," in *this proceedings*, 2010.
7. H.-P. Schlenvoigt, K. Haupt, A. Debus, F. Budde, O. Jäckel, S. Pfotenhauer, H. Schwoerer, E. Rohwer, J. G. Gallacher, E. Brunetti, R. P. Shanks, S. M. Wiggins, and D. A. Jaroszynski, *Nature Phys.* **4**, 130 (2008).
8. M. Fuchs, R. Weingartner, A. Popp, Z. Major, S. Becker, J. Osterhoff, I. Cortrie, B. Zeitler, R. Horlein, G. D. Tsakiris, U. Schramm, T. P. Rowlands-Rees, S. M. Hooker, D. Habs, F. Krausz, S. Karsch, and F. Grüner, *Opt. Expr.* **10**, 1425 (2002).
9. M. L. Ponds, Y. Feng, J. M. J. Madey, and P. G. O'Shea, *Nuc. Inst. Meth. Phys. Research A* **375**, 136 (1996).
10. M. S. Bakeman, C. B. Schroeder, K. E. Robinson, C. Toth, K. Nakamura, W. M. Fawley, and W. P. Leemans, *AIP Conference Proceedings* **1086**, 643–648 (2009), URL `http://link.aip.org/link/?APC/1086/643/1`.
11. J. G. Gallacher, M. P. Anania, E. Brunetti, F. Budde, A. Debus, B. Ersfeld, K. Haupt, M. R. Islam, O. Jäckel, S. Pfotenhauer, A. J. W. Reitsma, E. Rohwer, H.-P. Schlenvoigt, H. Schwoerer, R. P. Shanks, S. M. Wiggins, and D. A. Jaroszynski, *Phys. Plasmas* **16**, 093102 (2009).
12. K. Nakamura, W. Wan, N. Ybarrolaza, D. Syversrud, J. Wallig, and W. P. Leemans, *Rev. Sci. Instrum.* **79**, 053301 (2008).
13. W. P. Leemans, B. Nagler, A. J. Gonsalves, C. Tóth, K. Nakamura, C. G. R. Geddes, E. Esarey, C. B. Schroeder, and S. M. Hooker, *Nature Phys.* **2**, 696 (2006).
14. M. S. Bakeman, J. van Tilborg, T. Sokollik, D. Baum, N. Ybarrolaza, R. Duarte, C. Tóth, and W. P. Leemans, Calibration of a microchannel plate based euv grazing incident spectrometer at the advanced light source (2010), submitted to Rev. Sci. Instrum.
15. D. Attwood, *Soft X-Rays and Extreme Ultraviolet Radiation: Principles and Applications*, Cambridge University Press, 2000.
16. T. Tanaka, and H. Kitamura, *J. Synch. Rad.* **8**, 1221 (2001).
17. M. S. Bakeman, J. van Tilborg, K. Nakamura, A. Gonsalves, J. Osterhoff, T. Sokollik, C. Lin, K. E. Robinson, C. B. Schroeder, C. Tóth, R. Weingartner, F. Grüner, E. Esarey, and W. P. Leemans, "Undulator-Based Laser Wakefield Accelerator Electron Beam Energy Spread and Emittance," in *this proceedings*, 2010.
18. D. Thorn, C. G. R. Geddes, N. H. Matlis, G. R. Plateau, e. Esarey, M. Battaglia, C. B. Schroeder, S. Shiraishi, T. Stoehlker, C. Tóth, and W. P. Leemans, Spectroscopy of betatron radiation emitted from laser-produced wakefield accelerated electrons (2010), submitted to Rev. Sci. Instrum.
19. S. Kneip, S. R. Nagel, C. Bellei, N. Bourgeois, A. E. Dangor, A. Gopal, R. Heathcote, S. P. D. Mangles, J. R. Marquès, A. Maksimchuk, P. M. Nilson, K. T. Phuoc, S. Reed, M. Tzoufras, F. S. Tsung, L. Willingale, W. B. Mori, A. Rousse, K. Krushelnick, and Z. Najmudin, *Phys. Rev. Lett.* **100**, 105006 (2008).
20. A. Rousse, K. T. Phuoc, R. Shah, A. Pukhov, E. Lefebvre, V. Malka, S. Kiselev, F. Burgy, J.-P. Rousseau, D. Umstadter, and D. Hulin, *Phys. Rev. Lett.* **93**, 135005 (2004).
21. G. R. Plateau, C. G. R. Geddes, D. B. Thorn, N. H. Matlis, D. Mittelberger, T. Stoehlker, M. Battaglia, T. S. Kim, E. Cormier-Michel, K. Nakamura, E. Esarey, and W. P. Leemans, "X-ray Emission from Electron Betatron Motion in a Laser-Plasma Accelerator," in *this proceedings*, 2010.
22. A. L. Cavalieri, D. M. Fritz, S. H. Lee, P. H. Bucksbaum, D. A. Reis, J. Rudati, D. M. Mills, P. H. Fuoss, G. B. Stephenson, C. C. Kao, D. P. Siddons, D. P. Lowney, A. G. MacPhee, D. Weinstein, R. Falcone, R. Pahl, J. Als-Nielsen, C. Blome, S. Duĺsterer, R. Ischebeck, H. Schlarb, H. Schulte-Schrepping, T. Tschentscher, J. Schneider, O. Hignette, F. Sette, K. Sokolowski-Tinten, H. N. Chapman, R. Lee, T. N. Hansen, O. Synnergren, J. Larsson, S. Techert, J. Sheppard, J. S. Wark, M. Bergh, C. Caleman, G. Huldt, D. van der Spoel, N. Timneanu, J. Hajdu, R. A. Akre, E. Bong, P. Emma, P. Krejcik, J. Arthur, S. Brennan, K. J. Gaffney, A. M. Lindenberg, K. Luening, , and J. B. Hastings, *Phys. Rev. Lett.* **94**, 114801 (2005).
23. S. Jamison, G. Berden, P. J. Phillips, W. A. Gillespie, and A. M. MacLeod, *Appl. Phys. Lett.* **96**, 231114 (2010).
24. C. B. Schroeder, E. Esarey, J. van Tilborg, and W. P. Leemans, *Phys. Rev. E* **69**, 016501 (2004).
25. N. H. Matlis, G. R. P. J. van Tilborg, and W. P. Leemans, Single-shot spatiotemporal measurements of ultrashort thz waveforms using temporal electric-field cross-correlation (2010), accepted J. Opt. Soc. Am. B.
26. J. van Tilborg, C. B. Schroeder, C. V. Filip, C. Tóth, C. G. R. Geddes, G. Fubiani, R. Huber, R. A. Kaindl, E. Esarey, and W. P. Leemans, *Phys. Rev. Lett.* **96**, 014801 (2006).
27. W. P. Leemans, C. G. R. Geddes, J. Faure, C. Tóth, J. van Tilborg, C. B. Schroeder, E. Esarey, G. Fubiani, D. Auerbrach, B. Marcelis, M. A. Carnahan, R. A. Kaindl, J. Byrd, and M. C. Martin, *Phys. Rev. Lett.* **91**, 074802 (2003).
28. J. van Tilborg, C. B. Schroeder, C. V. Filip, C. Tóth, C. G. R. Geddes, G. Fubiani, E. Esarey, and W. P. Leemans, *Phys. Plasmas* **13**, 056704 (2006).
29. Z. Jiang, and X.-C. Zhang, *Appl. Phys. Lett.* **72**, 1945 (1998).
30. F. G. Sun, Z. Jiang, and X.-C. Zhang, *Appl. Phys. Lett.* **73**, 2233 (1998).
31. J. R. Fletcher, *Opt. Expr.* **10**, 1425 (2002).
32. X.-Y. Peng, O. Wiili, M. Chen, and A. Pukhov, *Opt. Express* **16**, 12342 (2008).
33. S. Jamison, J. Shen, A. M. MacLeod, W. A. Gillespie, and D. A. Jaroszynski, *Opt. Lett.* **28**, 1710 (2003).
34. J. van Tilborg, C. B. Schroeder, C. Tóth, C. G. R. Geddes, E. Esarey, and W. P. Leemans, *Opt. Lett.* **32**, 313 (2007).
35. Z. Jiang, and X.-C. Zhang, *Opt. Express* **5**, 243 (1999).

DISCLAIMER